Molecular Therapy
Original Article

Treatment with Recombinant Human MG53 Protein Increases Membrane Integrity in a Mouse Model of Limb Girdle Muscular Dystrophy 2B

Liubov V. Gushchina,[1] Sayak Bhattacharya,[1] Kevin E. McElhanon,[1] Jin Hyuk Choi,[1] Heather Manring,[1] Eric X Beck,[1] Jenna Alloush,[1] and Noah Weisleder[1]

[1]Department of Physiology and Cell Biology, Dorothy M. Davis Heart and Lung Research Institute, The Ohio State University Wexner Medical Center, Columbus, OH 43210-1252, USA

Limb girdle muscular dystrophy type 2B (LGMD2B) and other dysferlinopathies are degenerative muscle diseases that result from mutations in the dysferlin gene and have limited treatment options. The dysferlin protein has been linked to multiple cellular functions including a Ca^{2+}-dependent membrane repair process that reseals disruptions in the sarcolemmal membrane. Recombinant human MG53 protein (rhMG53) can increase the membrane repair process in multiple cell types both in vitro and in vivo. Here, we tested whether rhMG53 protein can improve membrane repair in a dysferlin-deficient mouse model of LGMD2B (B6.129-*Dysf*^{tm1Kcam}/J). We found that rhMG53 can increase the integrity of the sarcolemmal membrane of isolated muscle fibers and whole muscles in a Ca^{2+}-independent fashion when assayed by a multi-photon laser wounding assay. Intraperitoneal injection of rhMG53 into mice before acute eccentric treadmill exercise can decrease the release of intracellular enzymes from skeletal muscle and decrease the entry of immunoglobulin G and Evans blue dye into muscle fibers in vivo. These results indicate that short-term rhMG53 treatment can ameliorate one of the underlying defects in dysferlin-deficient muscle by increasing sarcolemmal membrane integrity. We also provide evidence that rhMG53 protein increases membrane integrity independently of the canonical dysferlin-mediated, Ca^{2+}-dependent pathway known to be important for sarcolemmal membrane repair.

INTRODUCTION

Dysferlinopathies are a heterogeneous group of degenerative muscle disorders associated with autosomal recessive inheritance that exhibits full deficiency or mutations in the gene encoding dysferlin (DYSF) protein. Dysferlin-deficient patients may show heterologous phenotypic progression of muscle wasting and weakness, with no clear correlation between their specific mutations and the onset or severity of muscle weakness. Recently, dysferlinopathies were divided into four main clinical types: limb girdle muscular dystrophy type 2B (LGMD2B) with primarily proximal weakness,[1–4] Miyoshi myopathy (MM) with primarily distal weakness,[3,4] distal myopathy with anterior tibial onset (DMAT),[2] and proximodistal weakness, which can include the symptom combinations described above.[1–4] LGMD2B is the most frequently diagnosed type of dysferlinopathy and it affects approximately 1 in 100,000–200,000 male and female patients, with a mean age of onset at around 26 years.[5–7]

Current treatments for LGMD are limited, and proposed therapeutic approaches are palliative and intended to allow patients to remain mobile as long as possible.[6,8–10] However, to our knowledge, none of these treatments has any effect on the underlying pathology. While possible future therapies for LGMD (including gene therapy replacement of affected genes[11,12] and the use of stem cells[13–15]) hold promise, these treatments are still years away from application in human patients. Genetic replacement approaches are further complicated by the number of different genes compromised in other LGMDs. As a result, there is a great need for intermediate therapies to reduce the pathology associated with LGMD and other muscular dystrophies. Potentially, a therapeutic agent would be more viable if it could treat multiple forms of LGMD by targeting a shared conserved pathologic mechanism in these distinct diseases.

Human dysferlin is a 237-kDa (2,080-amino-acid) transmembrane Ca^{2+}-binding protein that belongs to the ferlin family and localizes to the plasma membrane and t tubules of skeletal muscle fibers.[16,17] Various studies indicate that dysferlin contributes to plasma membrane repair in cultured myoblasts and in skeletal and cardiac muscles.[12,17–21] Plasma membrane repair is an active process in which multiple cellular mechanisms contribute to restoring membrane integrity following a break in the plasma membrane,[22–24] including when exocytotic intracellular vesicles traffic to sites of membrane disruption to form a repair patch.[25] Additional studies link dysferlin function to related cellular activities, including cell survival, regulation of endo- and exocytosis, vesicle fusion, trafficking, and

Received 16 August 2016; accepted 28 June 2017;
http://dx.doi.org/10.1016/j.ymthe.2017.06.025.

Correspondence: Noah Weisleder, PhD, Department of Physiology and Cell Biology, Dorothy M. Davis Heart and Lung Research Institute, The Ohio State University Wexner Medical Center, 473 W. 12th Avenue, Columbus, OH 43210-1252, USA.
E-mail: noah.weisleder@osumc.edu

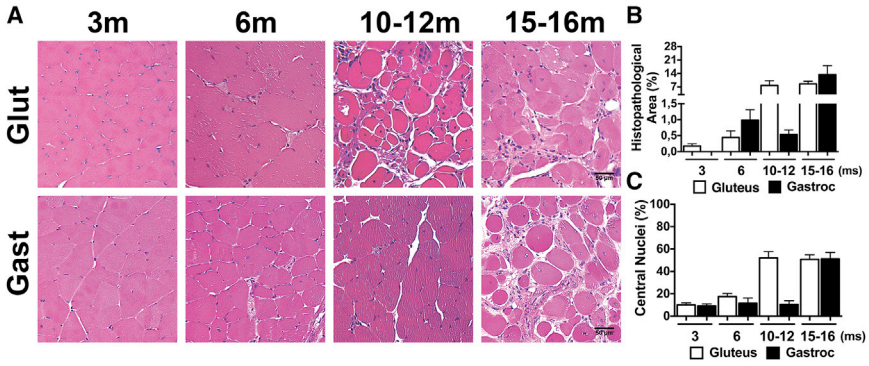

Figure 1. Histological Features of Muscular Dystrophy in *Dysf*$^{-/-}$ Mice

(A) H&E-stained histological sections from the gastrocnemius (Gast) and gluteus (Glut) muscle of *Dys*$^{-/-}$ mice at 3, 6, 10–12, and 15–16 months of age. Scale bars represent 50 μm. (B and C) Quantification analysis of H&E-stained sections from the indicated muscles displaying the percentage of (B) histopathological area and (C) central nuclei in the gastrocnemius and gluteus muscle of *Dysf*$^{-/-}$ mice at 3, 6, 10–12, and 15–16 months (ms) of age. Data are means ± SEM (n = 3–6 mice).

excitation-contraction coupling.[26–34] Interestingly, the histopathological examinations of cardiac[20,35–37] and skeletal muscles[12,38] from dysferlin-deficient mice suggest the existence of an alternative dysferlin-independent pathway for the cellular membrane repair process in cardiac cells.[39]

Different dysferlin-deficient mouse models of LGMD2B and related dysferlinopathies have been created and characterized.[40] Two mouse strains, SJL/J and A/J, contain spontaneous mutations in the dysferlin gene. The SJL/J spontaneous model of LGMD2B and MM harbors a mutation where the C2E dysferlin domain[38,41] encoded by exon 45 has been removed.[42,43] The A/J model,[38] generated by insertion of an ETn retrotransposon at intron 4 of the dysferlin gene, shows slower progression of muscular dystrophy than the SJL/J. However, both models demonstrate a mild phenotype in the development of muscle pathology, which complicates their use in research. The need for a genetically engineered and backcrossed mouse model lead to the generation of various mouse models, including *Dysf*$^{-/-}$ mice (B6.129-Dysf^{tm1Kcam}/J), B6.129S6-Dysf$^{tm2.1Kcam}$/J, B10.SJL-Dysf^{im}/AwaJ mice, *Dysf*$^{-/-}$ (129-Dysf^{tm1KCam}/J), and others.[18,38,40,43,44] The B6.129-Dys^{ftm1Kcam}/J mouse is the result of the deletion of a 12-kb genomic region, which corresponds to human exons 53–55 (1,983–2,080 amino acids), that encode the transmembrane domain of the dysferlin protein.

Recent studies identified additional molecular components of the membrane repair process, particularly those involved in a pathway thought to be specific to striated muscles.[45] Previous discoveries from our laboratory group and collaborators demonstrated that mitsugumin 53 (MG53), a muscle-enriched tripartite motif (TRIM) family protein[46] also known as TRIM72, is an essential component of the cell membrane repair machinery in striated muscle.[47–53] To reseal disruptions in cellular membranes, dysferlin-containing vesicles can be recruited by oligomerized MG53 protein that localizes on an intracellular membrane. MG53 oligomerization is presumably promoted by the changes in the oxidation state that occurs during acute membrane disruption between the intracellular and extracellular spaces from reduced to oxidized states.[48] While MG53 is an important driver of the membrane repair mechanism, targeting this process to treat LGMD requires a method that directly modulates the membrane repair capacity in skeletal muscle fibers. We previously found that recombinant human MG53 protein (rhMG53) can be directly applied to cells and tissues to increase the integrity of the plasma membrane in muscle and non-muscle cells.[54] This exogenously applied rhMG53 can interact with the plasma membrane at disruption sites and increase the resealing of the membrane both in vitro and in vivo with a mouse model of Duchenne muscular dystrophy.

In this study, we assess the therapeutic potential of rhMG53 administration to prevent muscle damage following eccentric exercise in the B6.129-Dys^{ftm1Kcam}/J dysferlin-deficient mouse model of LGMD2B. This dysferlin-deficient model does not show any dysferlin expression in skeletal tissues and thus can be used to study the pathology associated with LGMD2B and the therapeutic effects of rhMG53. These rhMG53-treated *Dysf*$^{-/-}$ mice displayed improved skeletal muscle fiber integrity in response to laser-induced damage and decreased release of biomarkers of muscle injury following in vivo muscle injury. Taken together, our data demonstrate that rhMG53 improves muscle fiber survival and suggest that this protein therapy may be beneficial for patients with LGMD2B.

RESULTS

Histopathological Characteristics of Muscular Dystrophy in Dysferlin-Deficient Mice

Numerous publications report a slow progression of muscle pathology in dysferlin-deficient mice that can occur in different timescales in different dysferlin-deficient mouse lines.[18,55–57] Thus, to assess the rate of development of muscle pathology in the B6.129-Dysf^{tm1Kcam}/J (*Dysf*$^{-/-}$) mice, we conducted a histological study in mice aged 3–15 months. Paraffin-embedded gastrocnemius (gastroc) and gluteus muscle cross-sections were stained with H&E (Figure 1A). By the age of 3 months (Figure 1A), an increase in muscle fibers with internal nuclei was detected in dysferlin null samples. Previous studies reported that most pathological characteristics of muscular dystrophy could be identified in skeletal muscle of dysferlin-deficient mice aged 4 and 8 months.[18,58,59] In our hands, we found that at age 6 months (Figure 1A), this strain of *Dysf*$^{-/-}$ mice demonstrated mild defects that included common fibers with central nuclei and limited histopathological areas. Between 6 and 10 months (Figure 1A), the *Dysf*$^{-/-}$ mice developed progressive muscular dystrophy

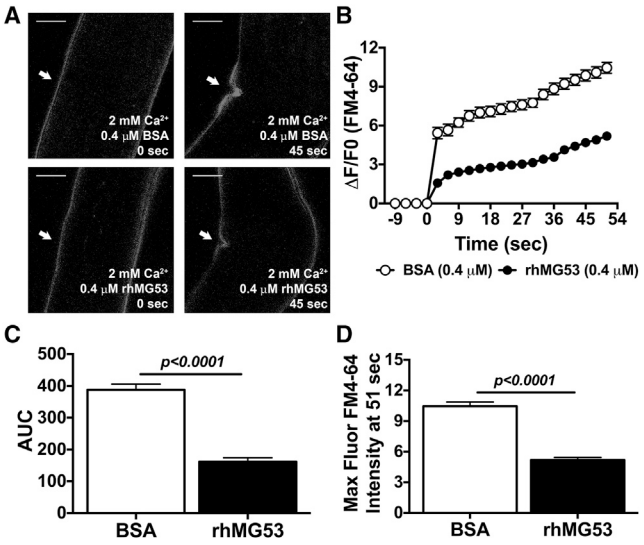

Figure 2. Ex Vivo Studies of rhMG53 Efficacy on Single FDB Fibers Derived from *Dysf*$^{-/-}$ Mice

(A) Representative images. (B and C) Time-dependent accumulation of FM4-64 dye (B) and the area under the curve (AUC) (C) demonstrate that rhMG53 protein efficiently accelerates membrane resealing in the micromolar concentration range on individual fibers damaged by an infrared laser. (D) The maximum fluorescence intensity indicates the mean peak value at 51 s seen for the FM4-64 signal in each group over the course of the experiment. White arrows indicate a wounding site at 0 and 45 s after laser injury. Scale bars represent 10 μm. Data are means ± SEM (n = 10–17). The Student's t test was used for statistical analysis.

with extensive symptoms, including extensive fibrosis and the majority of muscle fibers containing central nuclei. Quantification of these events in *Dysf*$^{-/-}$ mice at different ages indicated a significant increase in histopathological area and centrally located nuclei in myofibers at 6–10 months and older compared to 3- to 6-month-old *Dysf*$^{-/-}$ mice (Figures 1B and 1C; complete statistics appear in Table S1). The morphological changes were more pronounced in the gluteus compared with other skeletal muscles, as expected from previous studies. Thus, the development of pathology in these dysferlin-deficient animals was relatively similar to those shown in previously published studies in other dysferlin-deficient animals.

Exogenous Application of rhMG53 Increases Membrane Integrity Ex Vivo in a Ca^{2+}-Independent Manner

Since previous studies indicate that muscle fibers from dysferlin-deficient animals display compromised membrane repair,[18] we tested whether increasing membrane repair capacity could have protective effects in the *Dysf*$^{-/-}$ mouse model. One approach to increase membrane repair is through providing additional rhMG53 to isolated cells or through injection into experimental animals.[54,60] Lyophilized recombinant human MG53 (rhMG53) with greater than 97% purity based on high-performance liquid chromatography (HPLC) was reconstituted into physiological saline solution and its capacity as a protein agent was tested in resealing membrane disruption experiments. Complete flexor digitorum brevis (FDB) muscles and enzymatically isolated individual muscle fibers from *Dysf*$^{-/-}$ mice were damaged using infrared multi-photon laser microscopy. Internalized FM4-64 dye entry was used to determine membrane integrity in these muscle fibers. FM4-64 dye shows poor fluorescence in the aqueous solution outside the cell, with increased fluorescence once it enters the cell and binds lipids. When the membrane reseals, dye entry will cease and the fluorescent signal stabilizes. While these experiments are typically done on isolated muscle fibers, we developed an approach using whole FDB muscles that allows for these measurements to be made in a more native environment where the extracellular matrix surrounding the muscle fiber remains intact. We conducted comparative studies to determine differences in the response to these two approaches. In the individual FDB fibers we found that injury to the membrane results in local contraction of the fiber at the injury site (Figure 2A), as has been observed previously by multiple laboratories.[18,48,50,61,62] rhMG53 protein applied to the external solution in the presence of Ca^{2+} showed reduced dye entry compared to the equimolar BSA protein control (Figures 2A and 2B). Moreover, the maximum intensity of FM4-64 fluorescence is considerably less for the rhMG53 group versus the BSA group. To quantify the differences, we calculated the total area under the curve (AUC) (Figure 2C), a useful tool for estimating the bioactivity of protein drugs, and the maximum intensity of FM4-64 dye uptake for the curve (Figure 2D) for both the rhMG53 and BSA groups. We determined that individual dysferlin-deficient fibers in the presence of rhMG53 and Ca^{2+} reduced the FM4-64 dye entry into the muscle fiber, as we previously observed.[54] These results indicate that externally delivered rhMG53 protein significantly increases the integrity of a disrupted plasma membrane.

In contrast to the isolated FDB muscle fibers, the multi-photon laser injury to muscle fibers in an intact FDB muscle does not produce the localized contraction that distorts the muscle fiber (Figures 3A and 3B). Thus, we used this methodology to test the effects of rhMG53 on these muscle preparations to determine the Ca^{2+} dependence of rhMG53 function. Previous studies demonstrated the essential role of Ca^{2+} in vesicle trafficking and vesicle fusion that leads to membrane repair in many model systems.[18,48,61] We then tested whether BSA, saline, or rhMG53 and Ca^{2+} concentration in the extracellular solution affects the sarcolemma repair process in the intact FDB muscle from *Dysf*$^{-/-}$ mice. We conducted muscle laser injury experiments with the Tyrode solution calcium concentration at 0 or 2.0 mM (Figures 3A and 3B). In the presence of either BSA or saline, 0 or 2.0 mM extracellular Ca^{2+} resulted in no significant changes in FM4-64 dye influx (Figures 3A and 3C). This similar response with and without extracellular Ca^{2+} would be expected in these muscle fibers, since the loss of membrane repair capacity in *Dysf*$^{-/-}$ muscle leads to a similar level of dye entry under both conditions.[18] This contrasts with the response seen in C57BL/6J WT mouse muscles, where the membrane efficiently reseals in the presence of extracellular Ca^{2+} and removal of extracellular Ca^{2+} significantly increases dye influx following laser wounding (Figures 3D and 3E).

Addition of rhMG53 to the external solution decreased the FM4-64 dye influx into the *Dysf*$^{-/-}$ muscle fibers within FDB muscles

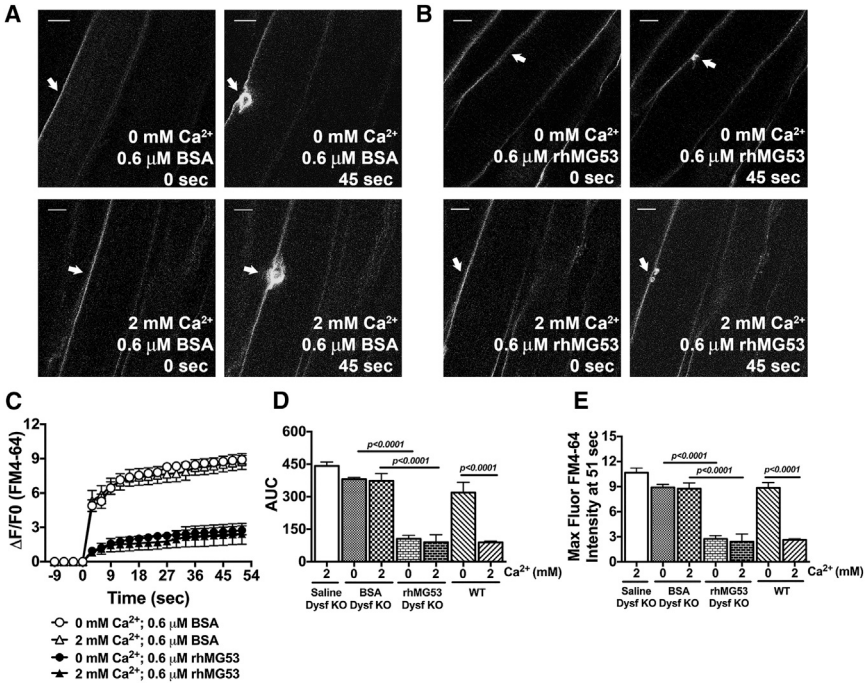

Figure 3. Ex Vivo Studies of rhMG53 Efficacy on Whole FDB Muscle Derived from *Dysf*$^{-/-}$ Mice

(A–C) Representative images (A and B) and time-dependent accumulation of FM4-64 dye in whole FDB muscles from *Dysf*$^{-/-}$ (C). White arrows indicate the wounding site at 0 and 45 s after laser injury. Scale bars represent 10 μm. (D) The area under the curve (AUC) of FM4-64 fluorescence traces display the membrane-resealing process in the presence of saline-only and BSA protein (as controls) and rhMG53 on the intact skeletal muscle in the presence and absence of calcium ions. (E) The maximum fluorescence intensity (MaxFluor) at 51 s post-injury closely follows the AUC measurements. AUC and MaxFluor FM4-64 values of sedentary C57BL/6J (WT) mice are provided to display the contribution of dysferlin deficiency on those parameters and the Ca^{2+}-independent manner of rhMG53 function. Data are means ± SEM (n = 4–12). The Tukey-ANOVA test was utilized for statistical analysis.

following laser injury. Interestingly, rhMG53 produced the same increase in membrane repair in either a 0 mM or 2.0 mM Ca^{2+} environment (Figures 3B and 3C). This suggests that while the canonical membrane repair process requires extracellular Ca^{2+}, the effect of rhMG53 on membrane repair is not dependent on the presence of extracellular Ca^{2+} in *Dysf*$^{-/-}$ muscle fibers. Quantitative analysis of these changes in dye influx (Figures 3D and 3E; Table S2) shows an approximately 72%–80% and 68%–77% decrease of total AUC and maximum fluorescence intensity for rhMG53-treated *Dysf*$^{-/-}$ muscles compared to BSA and saline either in the absence and presence of extracellular Ca^{2+}, respectively.

rhMG53 Reduces Release of Serum Markers of Eccentric Exercise-Induced Injury in Dysferlin-Deficient Mice

Since the *Dysf*$^{-/-}$ mice show mild histopathology at an early age, we accelerated the cellular membrane disruptions in muscle fibers[63] using acute treadmill exercise to establish whether rhMG53 treatment might improve muscle membrane integrity in vivo. For these studies, 3-month-old *Dysf*$^{-/-}$ mice were randomly separated into three groups: a sedentary (control) group and two exercise groups where animals received either saline or 5 mg/kg rhMG53 intraperitoneal (i.p.) injections before exercise. The exercise groups of mice began running 1 hr after injection on a downhill treadmill (−15° angle) for 40–45 min at a speed of 18 m/min. Serum creatine kinase (CK) and lactate dehydrogenase (LDH) profiles, as markers of muscle cell damage and tissue injury due to disease or trauma,[64] were used to assess the extent of sarcolemmal membrane disruption. Levels of both enzymes increased with the eccentric contractions produced during treadmill running.[65–68] Serum levels of both CK (Figure 4A) and LDH (Figure 4B) were significantly elevated in response to downhill exercise in both saline- and rhMG53-treated groups versus control group. However, exercised *Dysf*$^{-/-}$ mice receiving a single dose of rhMG53 showed significantly reduced serum CK (~22%) and LDH (~20%) levels compared to the saline-treated group. To evaluate the contribution of dysferlin deficiency that may lead to an elevation in muscle markers level, both CK and LDH were also measured in the serum of C57BL/6J (WT) mice. Compared to WT mice, observed serum CK and LDH levels increased approximately 230% and 39% respectively in the control (sedentary) *Dysf*$^{-/-}$ group (Figures 4A and 4B; Table S3).

Levels of MG53 Accumulation in Skeletal Muscle Tissues

We next confirmed rhMG53 availability and its distribution in the striated muscle. To confirm the presence of rhMG53 in the serum samples collected for measurement of CK and LDH, we used western blotting for MG53 (Figure 4C). We observed a nonspecific band in all lanes, the size of which is well correlated with serum albumin, and only exogenously delivered rhMG53 protein in its monomeric and oligomeric (Figure 4C, top) forms that have been previously shown to be involved in MG53 function.[69] The level of rhMG53 was significantly elevated above the endogenous MG53 serum levels,[54,70] with the endogenous MG53 level only detected in over-exposed blots.

We also tested the amount of total MG53 protein that accumulated in the skeletal muscle following injection of rhMG53 (Figure 5). Exogenously delivered rhMG53 protein in two different skeletal muscles did not display any bands representing oligomeric forms such as those observed in serum samples. We then compared whether total MG53 expression in *Dysf*$^{-/-}$ mice and WT mice is changed in response to exercise and protein treatment in gluteus and gastroc tissue extracts (Figures 5A and 5C). We observed a slight and

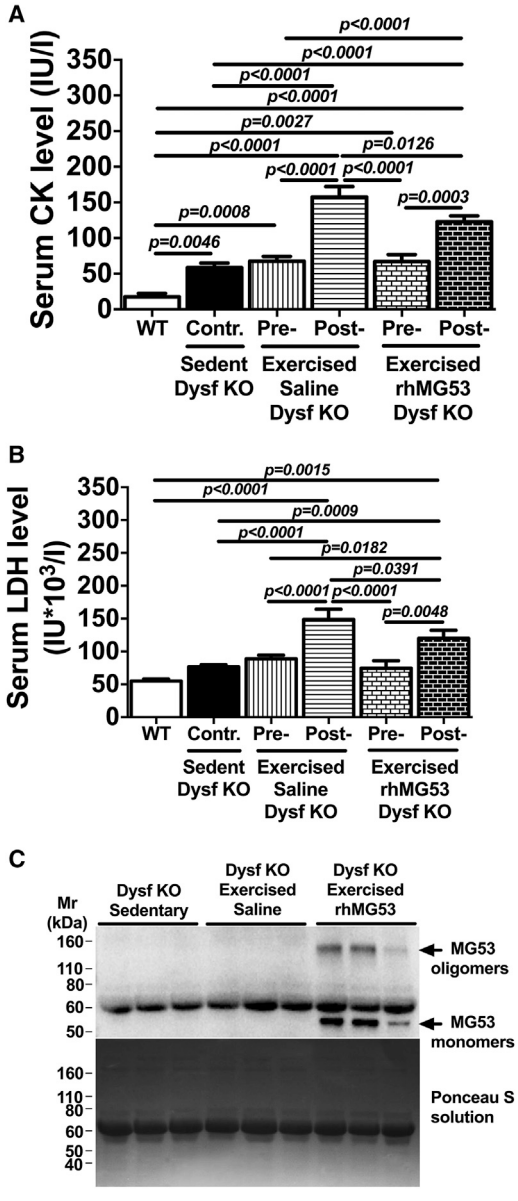

Figure 4. Effect of rhMG53 Treatment on Serum Markers in *Dysf*$^{-/-}$ Mice in Response to Eccentric Exercise

(A and B) Creatine kinase (CK) (A) and LDH (B) levels after eccentric exercise demonstrate rhMG53 efficacy as a protein drug to prevent muscle disruptions. CK and LDH levels in serum of sedentary C57BL/6J (WT) mice show the contribution of dysferlin deficiency on those cellular markers. Control mice (Contr) are considered to be sedentary *Dysf*$^{-/-}$ (KO) mice. These were compared with exercised *Dysf*$^{-/-}$ mouse serum samples. (C) Western blot of serum from *Dysf*$^{-/-}$ mice shows nonspecific MG53 bands and i.p. delivered rhMG53 protein level in eccentric exercised rhMG53-treated group (top). The higher molecular weight MG53 oligomers (indicated by black arrows) were detected only in the rhMG53-treated group. The Ponceau S solution blot displays that similar amounts of serum proteins were loaded in the gel and then transferred to a PVDF membrane (bottom of C). Data are means ± SEM (n = 6 for A and B; n = 3 for C). The Benjamini, Krieger, and Yekutieli ANOVA test was used for statistical analysis.

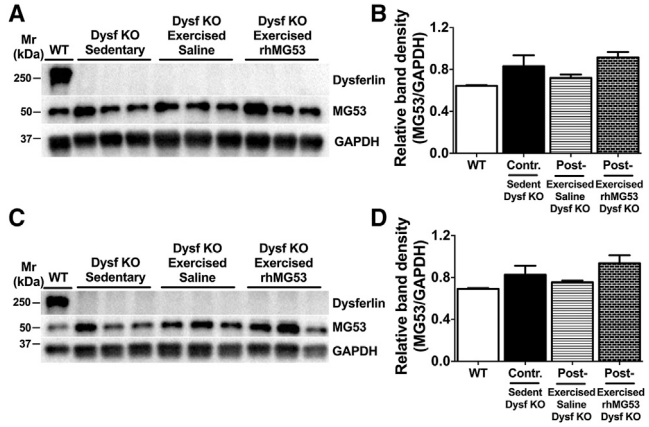

Figure 5. Western Blot Analysis of Dysferlin and MG53 Protein Expression in Striated Muscle Tissue from Wild-Type and *Dysf*$^{-/-}$ Mice

(A and C) Western blots of dysferlin and MG53 levels in whole gluteus (A) and gastrocnemius (C) tissue extracts, and glyceraldehyde 3-phosphate dehydrogenase (GAPDH) as a control, from C57BL/6J (WT, lane 1) and *Dysf*$^{-/-}$ mice (sedentary group, lanes 2–4; exercised saline-treated group, lanes 5–7; exercised rhMG53-treated group, lanes 8–10). (B and D) Densitometric analysis of the western blots presented in (A) and (C) was carried out using ImageJ software. The intensity of MG53 bands was normalized to the GAPDH band intensity of the respective sample. Data are means ± SEM (n = 3 for each group).

statistically insignificant increase in the level of MG53 protein in the muscle tissues of the injected mice (Figures 5B and 5D).

Injection of rhMG53 Improved Membrane Integrity in Dysferlin-Deficient Mice

To determine whether rhMG53 administration can improve sarcolemmal membrane integrity in muscle fibers damaged during downhill treadmill exercise, we stained histological sections from various muscles with fluorescent-labeled antibodies against mouse immunoglobulin G (IgG).[71] When IgG is detected in otherwise intact muscle fibers, it indicates a muscle fiber in which the membrane either has increased resistance to injury or has been broken and then resealed by membrane repair. If IgG is observed in muscle fibers without intact membranes, this suggests these may be necrotic fibers. Confocal microscopy shows that treadmill exercise increases the number of IgG-positive fibers in multiple muscle types from the *Dysf*$^{-/-}$ mouse hind limb (Figure 6A). Quantification of the number of IgG-positive fibers (Figures 6B–6D) showed a significant increase in IgG-positive fibers for the gluteus (~124%), extensor digitorum longus (EDL) (~23%), and soleus (~60%) muscles after exercise versus control sedentary *Dysf*$^{-/-}$ mice. However, the *Dysf*$^{-/-}$ mice injected with rhMG53 protein showed a considerable reduction in the number of IgG-positive fibers. The percentage of IgG-positive fibers was significantly lower for the gluteus (~26%), EDL (~12%), and soleus (~27%) muscles between the rhMG53- and saline-treated groups (Figures 6B–6D; Table S4).

Another method to evaluate cellular membrane permeability in vivo in *Dysf*$^{-/-}$ mice after exercise is the injection of Evans blue dye (EBD)

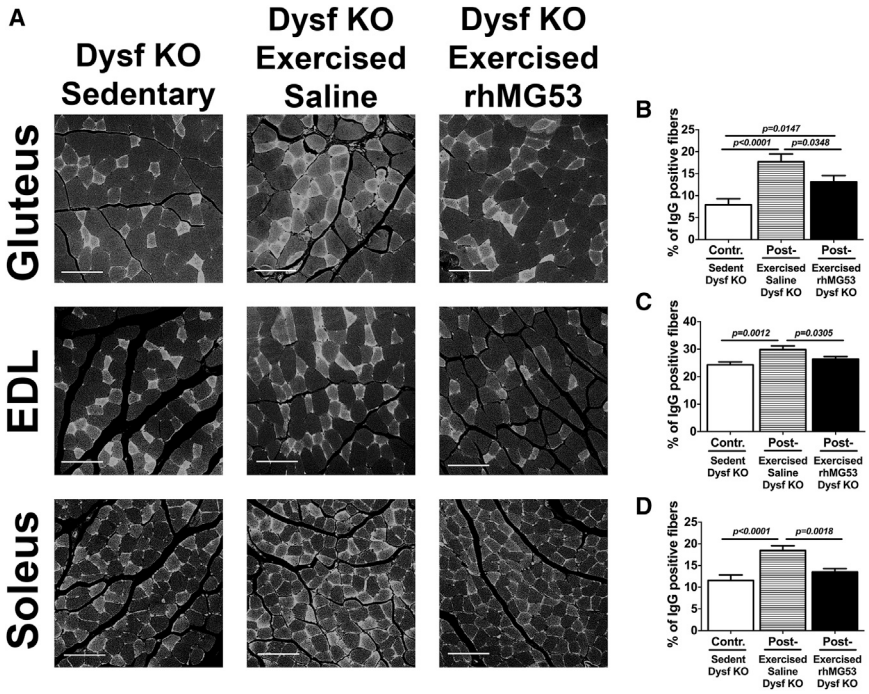

Figure 6. A Single Dose of rhMG53 Prevents Exercised-Induced Sarcolemmal Membrane Damage in *Dysf*$^{-/-}$ Mice

(A) Representative images of IgG staining. Paraffin sections of gluteus, EDL, and soleus muscle stained with fluorescent anti-mouse-IgG antibodies [IgG (H+L)] demonstrate the distribution of IgG-positive and IgG-negative fibers in selected skeletal muscles, showing the loss of membrane integrity in response to exercise and its improvement in the rhMG53-treated group. Scale bars represent 100 μm. (B–D) Quantification analysis of IgG-positive fibers for the gluteus (B), EDL (C), and soleus muscles (D). *Dysf*$^{-/-}$ mice show significant reductions in positive muscle fiber damage in the rhMG53-treated group relative to both the control and saline-treated groups. Data are means ± SEM (n = 6 for each group). The Benjamini, Krieger, and Yekutieli ANOVA test was used for statistical analysis.

as a marker to identify damaged skeletal muscle fibers.[72] At 18 hr post-EBD injection, *Dysf*$^{-/-}$ mice were injected with either saline or rhMG53 protein and exercised as described above. Following treadmill running, various muscles were collected and mounted as frozen histological sections or for extraction of EBD from the tissues. Confocal imaging of frozen sections from EDL and gastroc muscles (Figure 7A) showed increased EBD uptake into individual muscle fibers. To visualize the basement membrane of individual muscle fibers, EDL and gastroc sections were stained with laminin, followed by Alexa Fluor 488 (green)-labeled secondary antibody. EBD uptake was quantified by extraction from various muscles and measuring EBD differences by spectrophotometry (Figures 7B–7G). These results showed increased EBD uptake into the gluteus, soleus, EDL, tibialis anterior (TA), and gastroc skeletal muscles of *Dysf*$^{-/-}$ mice after a single downhill treadmill running regimen (Figures 7B–7F). We found that injection of rhMG53 reduced the amount of EBD in these muscles compared to the saline-treated group back to the levels seen in the unexercised *Dysf*$^{-/-}$ control mice, indicating that membrane repair might be effectively recovered in all presented types of muscle cells (Figures 7B–7F; Table S5). Since there is only limited damage to the FDB and diaphragm muscle from treadmill running, we also measured the EBD uptake in this muscle as a control and saw no significant increase in either muscle following exercise (Figure 7G and not shown). This shows the specificity of this approach for producing sarcolemmal membrane disruption of targeted muscles.

DISCUSSION

LGMD2B is a degenerative genetic muscle disease with limited treatment options for patients with this rare disorder. To date, proposed treatments for LGMD2B include Resolaris (a physiocrine-based protein product, which is in a phase Ib/II clinical trial; aTyr Pharma), adeno-associated virus (AAV)-mediated gene therapy based on target gene replacement[12] in dysferlin-deficient patients, and the potential use of stem cell regenerative medicine approaches. As LGMD2B patients currently lack effective treatment options, there is an unmet medical need for novel therapeutic approaches that can treat the underlying pathogenic mechanisms at work.

In this study, we demonstrate the therapeutic potential for rhMG53 protein to treat one of the underlying defects associated with LGMD2B. Previous studies showed that rhMG53 increased membrane repair in muscle and non-muscle cells when the cell is injured.[52,54,73] In this study, the effects of rhMG53 were established in ex vivo FDB muscle fibers and then in vivo on dysferlin-deficient mice using multiple experimental approaches. Our initial proof-of-concept studies used both isolated muscle fibers and whole FDB muscles injured by multi-photon microscopy. In both preparations, we found that dye entry decreased following laser injury when exogenous rhMG53 protein is present in the low micromolar range. Additionally, we found that whole muscles injured with multi-photon microscopy behaved differently than isolated, individual muscle fibers under the same conditions. While individual fibers show distension due to local contraction, muscle fibers within the bundle maintain their normal structure, possibly as a result of maintaining their extracellular connections within the native tissue. This may result in the variation in the kinetics of dye entry in these assays, where the individual muscle fibers show a longer phase of dye entry but the dye entry in fibers remaining in muscle bundles stabilizes shortly after injury. These results emphasize that the tissue environment is an important component of sarcolemmal membrane repair in native skeletal muscle through mechanism(s) that remain to be elucidated. It is also possible that there is a variation in the amount of membrane damage produced in these two preparations; however, the similar levels of

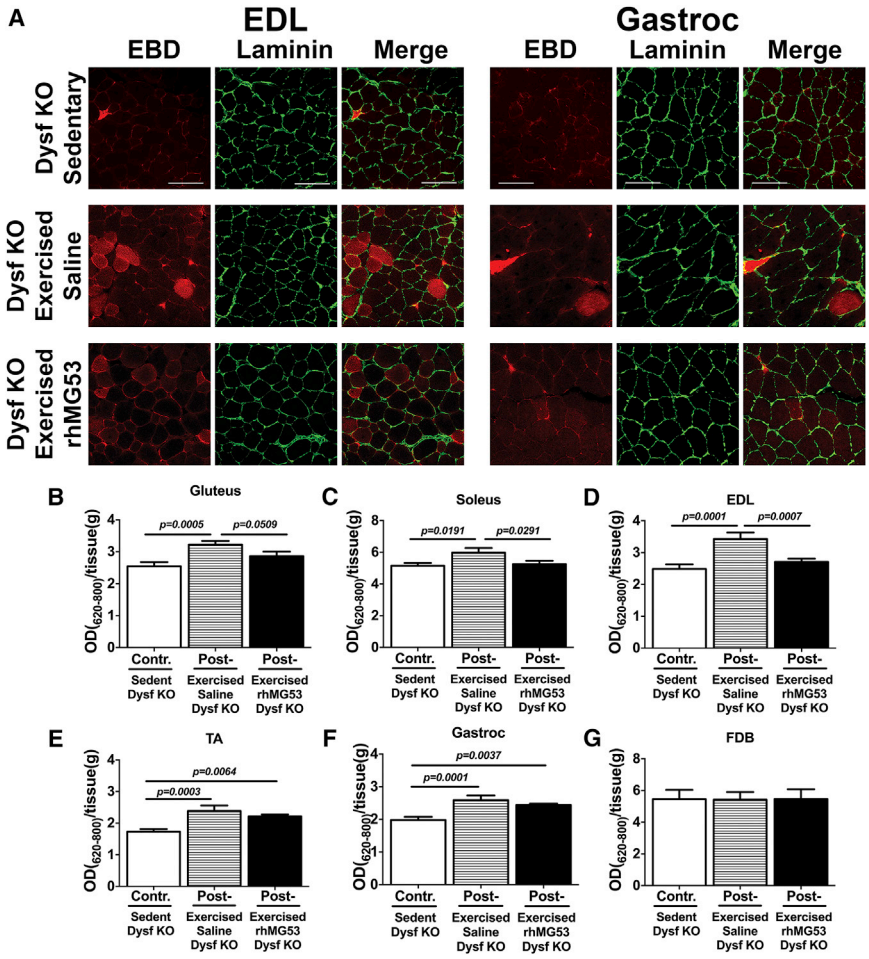

Figure 7. Effect of Acute rhMG53 Administration on Skeletal Muscle Membrane Permeability after Exhaustion Exercise in an LGMD2B Mouse Model

(A) Representative images of EBD uptake and laminin immunostaining in EDL (left) and gastrocnemius (Gastroc, right). Tissues harvested from the same *Dysf*$^{-/-}$ mice used for spectrophotometric quantification in (B) through (G). Scale bars represent 100 μm. (B–G) Quantification of EBD extraction from gluteus (B), soleus (C), EDL (D), TA (E), gastroc (F), and FDB (G) muscles from *Dysf*$^{-/-}$ mice. Measurements as duplicates. Data are means ± SEM (n = 6 for each group). The Benjamini, Krieger, and Yekutieli ANOVA test was used for statistical analysis.

total fluorescence signal and peak signal seen in the two preparations argue that similar levels of damage did occur. As expected, our studies confirmed that the *Dysf*$^{-/-}$ muscle fibers did not show differences in FM4-64 dye influx when Ca^{2+} was removed from the extracellular solution. This is in contrast to wild-type muscle fibers that show elevated dye entry in the absence of extracellular Ca^{2+} even with the complete muscle preparations used in these studies, which indicates that our use of whole muscles in this assay provides a reliable measurement of membrane repair. These results indicate that dysferlin-deficient muscle fibers fail to repair independently of Ca^{2+} entry, causing similar dye entry values for dysferlin-deficient fibers as the WT fibers injured in absence of Ca^{2+} (Figure 3).

We also found that the function of extracellularly delivered rhMG53 protein is not dependent on the presence of extracellular Ca^{2+} outside the muscle fiber. This is an interesting finding because the canonical cell membrane repair mechanism is thought to be dependent on extracellular Ca^{2+} entry into the cell.[25,48] Our data support that exogenous rhMG53 does not act through a Ca^{2+}-dependent process since it has identical effects on membrane repair when extracellular Ca^{2+} is removed from the external solution. These results suggest that while endogenous MG53 contributes to the trafficking of intracellular vesicles,[47,49,53] exogenous rhMG53 may function through a different mechanism. This may explain why rhMG53 can effectively increase membrane integrity in *Dysf*$^{-/-}$ muscle fibers when the canonical membrane repair process is disrupted due to the absence of dysferlin. While the specific mechanism targeted by rhMG53 is not yet clearly identified, it is possible that rhMG53 is interacting directly with the membrane lipids at the disruption site to assist in increasing membrane integrity or with resealing the injured membrane. One potential lipid target for the effect is phosphatidylserine, which binds with high affinity and specificity to rhMG53[47,48] and fragments of the MG53 protein.[48,74] Future studies will be necessary to resolve whether this lipid binding characteristic contributes to the function of rhMG53. These studies could help to establish whether rhMG53 acts through modulation of membrane repair or by increasing the resistance of the membrane to damage. Previous studies concluded that rhMG53 increased membrane repair when applied externally to multiple cell types[54,60]; however, the Ca^{2+}-insensitive nature of rhMG53 function found here suggests that direct effects on membrane integrity could also contribute to the function of rhMG53.

When we conducted our in vivo studies, we used the B6.129-*Dysf*^{tm1Kcam}/J (*Dysf*$^{-/-}$) mouse line as a model of LGMD2B. We found that this model shows similar progression of the dystrophic phenotype, as reported in other dysferlin-deficient mouse lines. Slow progression of the disease state is an advantage in modeling the human disease in some respects, since LGMD2B displays a relatively late age of onset and can progress slowly in many patients. In our in vivo proof-of-concept experiments, we chose to use a downhill treadmill running protocol to produce eccentric contractions in the hind limb muscles of these mice. Eccentric contractions increase the number of membrane disruptions that occur in these muscles, thus providing an opportunity to test the effects of rhMG53 on membrane

repair in this model. Injection of rhMG53 could minimize the release of CK and LDH into the external space through disruption in the sarcolemmal membrane. While CK is a more specific marker of muscle injury due to its muscle specific nature, the concurrent decrease in LDH release further supports that rhMG53 increases the integrity of the sarcolemmal membrane. We also found that two different histological assays of sarcolemmal membrane repair, IgG staining and EBD exclusion, support that rhMG53 increases membrane repair capacity in this LGMD2B mouse model. These results illustrate that multiple anatomical muscles can be effectively targeted to produce therapeutic effects at a level that can prevent the loss of membrane integrity produced by compromised membrane repair capacity. However, these acute studies are not sufficient to indicate that rhMG53 can prevent the development of pathology in the *Dysf*$^{-/-}$ mice. Establishing such therapeutic effects requires prolonged treatment with rhMG53 over the majority of the lifespan of the animal, as the pathology develops slowly in these mouse models.

Analysis of the levels of rhMG53 in serum and muscle tissues show that we can produce effective therapeutic levels in the serum that are in excess of the endogenous levels of MG53 previously reported.[54] It also appears that the endogenous levels of MG53 in *Dysf*$^{-/-}$ serum are lower than those previously observed in the *mdx* mouse model of Duchenne muscular dystrophy, which corresponds to the less severe pathology seen in the muscles of the *Dysf*$^{-/-}$compared to the *mdx* mouse. Oligomers of rhMG53 were also present in these serum samples as expected, since previous studies suggest that rhMG53 forms dimers or higher molecular weight oligomers through specific residues in the coiled-coil domain of the protein.[69] We also observed that only small quantities of rhMG53 appear to be necessary in the skeletal muscle in order to generate therapeutic effects in vivo, which would simplify the use of the recombinant protein for the treatment of neuromuscular diseases. It should be noted that more sensitive measurements of the extent of rhMG53 accumulation in skeletal muscle will be required to determine the pharmacodynamic relationship between rhMG53 and in vivo improvement of LGMD2B.

An additional factor to consider is that recent studies link dysferlin to other cellular processes aside from membrane repair.[75] One additional function that could contribute to the progression of LGMD2B is the role of dysferlin in the regulation of t-tubule structure and function in regulation of Ca^{2+} signaling in skeletal muscle. Dysferlin is known to localize to the t tubules[16,76] and studies link this localization to regulation of various cell functions. Loss of dysferlin can compromise the ability of muscle fibers to maintain t-tubule structures following stress[77] and to function properly in intracellular Ca^{2+} release pathways.[34] It is possible that native MG53 could also contribute to some of these cellular processes through its known interaction with dysferlin.[50] Indeed, recent studies link native MG53 to the regulation of t-tubule resident Ca^{2+} handing responses.[78] However, we have no data to show that the exogenous rhMG53 used in this study enters into the cell; thus, to our knowledge, there is no current evidence that rhMG53 acts directly on these other functions of dysferlin. While compromised membrane repair is one mechanism that can contribute to the progression of LGMD2B, these other functions linked to dysferlin can have pathologic consequences that could contribute to disease progression. Future studies should account for concerns that multiple pathogenic mechanisms could be at work in dysferlin-deficient muscle.

Taken together, our results provide in vitro and in vivo evidence that rhMG53 is effective in enhancing membrane integrity in a LGMD2B mouse model. The mechanism of action appears to increase the membrane integrity of skeletal muscle fibers to compensate for the inherent membrane repair defect seen in these animals. We also see that rhMG53 may increase membrane integrity by targeting a dysferlin-independent response that is not dependent on the presence of extracellular Ca^{2+}. Future studies will focus on the nature of this protective response and determine whether chronic treatment of mouse models of neuromuscular disease can minimize the pathology.

MATERIALS AND METHODS

C57BL/6J (WT) and one breeding pair of B6.129-*Dysf*^{tm1Kcam}/J (*Dysf*$^{-/-}$) mice were purchased from The Jackson Laboratory (stock number 013149) and were bred and maintained in standardized conditions at 22 ± 2°C under a 12-hr/12-hr light cycle (lights on at 7 a.m. EST). Genotypes of *Dysf*$^{-/-}$ mice were verified as described in the protocol available on The Jackson Laboratory's website (https://www2.jax.org/protocolsdb/f?p=116:5:0::NO:5:P5_MASTER_PROTOCOL_ID,P5_JRS_CODE:26269,013149). All experimental procedures were approved by The Ohio State University Institutional Animal Care and Use Committee. Animals were maintained in accordance with the recommendations of the NIH Guide for the Care and Use of Laboratory Animals.

Treadmill Exercise

At 3 months of age, *Dysf*$^{-/-}$ mice were randomly assigned into three groups: one sedentary (considered as control mice) group and two exercise groups (n = 6–9 per group). The two exercise groups were acclimated to the treadmill by moderate exercise training that included a series of downhill runs for 5 min at the speed of 8 m/min for 2 consecutive days. Exercised animals were injected i.p. once with either saline solution or 5 mg rhMG53/kg body weight. Saline injections were used to control for stress induced during i.p. injection. At 60–90 min after injection, the mice were exercised on an Exer-3/6 rodent treadmill (Columbus Instruments) at a 15° downward angle for 40–45 min at 18 m per min.[54] Mice were euthanized immediately after acute exercise and tissues were collected for analysis.

Tissue Sample Processing, Histopathology, and IgG Immunohistochemistry

The blood samples for baseline and post-exercise measurements were collected by cheek punch using a Goldenrod Animal Bleeding Lancet (Medipoint) and cardiac puncture, respectively. Serum was separated and used for measuring enzyme activity immediately after collection. The remaining serum was frozen and stored at −80°C for future analysis. Commercial enzyme activity kits were used to measure LDH (Takara Bio) and CK levels (Sekisui Diagnostics) using a

Flexstation3 plate reader (Molecular Devices) per the manufacturer's directions.

Tissues were harvested and fixed in 10% buffered formalin solution, which was replaced with 70% ethanol after 24 hr. Skeletal muscle tissues were embedded in paraffin and then blocked and microtome sectioned (5 μm) at the Pathology Core Facility at The Ohio State University Wexner Medical Center. All sections were deparaffinized and rehydrated in decreasing concentrations of ethanol. H&E (Thermo Scientific) staining was performed according to the manufacturer's instructions to visualize the extent of fibrosis in dystrophic skeletal muscle. Random images were collected on a Zeiss Axioplan microscope and then the number of myofibers with centrally located nuclei was determined by manual counting. The percentage of centralized nuclei was calculated as the number of fibers displaying internal nuclei divided by the total number of fibers in the cross-section of corresponding tissue (approximately 600–1,100 fibers/gluteus and 560–1,250 fibers/gastrocnemius). To quantify the percentage of total histopathological area in the muscles, ImageJ software (NIH) was used to manually highlight areas in collected images that showed the appearance of fibrosis and/or obvious infiltration of immune cells. In these measurements, any areas that showed separation of the tissue or another fixation artifact were not highlighted for analysis. The percentage area that contained immune cells or had a fibrotic appearance was calculated as that area divided by the total area of muscle tissue that appeared in the image.

Immunoglobulin G stain was used for intracellular IgG [IgG (H+L)] to determine muscle damage and fibrotic scarring. After dehydration, gluteus, EDL, and soleus muscle sections from all groups of mice were subjected to antigen retrieval using 1× Citra Plus (HK086-9K; BioGenex) solution and heated as described in the instruction manual and then stained with a 0.04% Alexa Fluor 488 goat anti-mouse IgG (A-11001; Life Technologies) solution in 2% BSA for 3 hr at room temperature, washed in PBS, and mounted with coverslips. Images for IgG staining were taken using an Olympus FluoView FV1000 confocal microscope. 4–10 region-of-interest images were consequently chosen for each muscle section. All images were analyzed using Olympus FV10-ASW 4.1 Viewer and ImageJ software. The IgG-positive and IgG-negative fibers were individually quantified and then calculated as a percentage of total fibers for each group.

Evans Blue Dye Uptake and Tissue Processing

EBD (Sigma-Aldrich), 1% in physiological saline (0.15 M NaCl, 10 mM phosphate buffer, pH 7.4), sterilized by passage through a 0.22-μm membrane filter was intravenously (i.v.) injected via the tail vein according to the mouse's body weight. 18 hr later, mice were injected i.v. with either saline or rhMG53, exercised, and euthanized as described above. The following skeletal muscles (gluteus, gastroc, soleus, TA, EDL, and FDB as a control) were bilaterally dissected and their individual mass weights were recorded. For some samples, frozen sections were cut using a Leica CM1510S cryostat (Leica Biosystems). Sections (10 μm) were fixed in methanol/acetone mixture (1:1 ratio) at −20°C for 4 min, washed in PBS solution, and incubated in 2% BSA in PBS solution (blocking buffer) for 30 min at room temperature. Sections were stained with antibody against laminin (1:500, rabbit polyclonal, ab11575; Abcam) for 3 hr at room temperature, washed in PBS, and incubated with a 0.04% Alexa Fluor 488 goat anti-rabbit IgG (H+L) (A-11034; Life Technologies) solution in blocking buffer for 2 hr at room temperature, washed in PBS, and mounted with coverslips. Images were made by an Olympus FluoView FV1000 confocal microscope using 546 nm for EBD and 488 nm for laminin excitation filters. To extract the EBD from the remaining samples, 1 mL formamide (47670, 250 mL; Sigma-Aldrich) was added to each tube and incubated at 55°C for 2 hr. After high-speed centrifugation for 5 min, the supernatants were collected and the absorbance of samples and formamide as the blank was read at 620 nm with subtraction background at 800 nm.

Western Blotting

Protein concentrations of extracts from mouse tissues were isolated and extracted as previously described.[54,79] Protein content was determined using BSA as a standard according to the Bradford assay. Protein samples (10–20 μg/lane) were separated by SDS-PAGE at room temperature on 4%–15% gradient gels at 120 V and were transferred to polyvinylidene difluoride (PVDF) membranes (Bio-Rad) through electroblotting. Blots were probed with antibodies against dysferlin (1:2,500, mouse monoclonal antibody), TRIM72/MG53 (1:2,500, custom rabbit polyclonal antibody), glyceraldehyde 3-phosphate dehydrogenase (GAPDH) (1:10,000, D16H11; Cell Signaling), and appropriate horseradish peroxidase (HRP)–conjugated secondary antibodies (1:5,000; Santa Cruz Biotechnology). The blots were developed using enhanced chemiluminescence (ECL) prime detection reagent (GE Healthcare). Bio-Rad Image Lab (version 4.1) and ImageJ software were used for blot analysis.

Laser-Induced Muscle Damage

The membrane injury assay was performed on both isolated FDB muscle fibers and intact muscle. The FDB muscle from male *Dysf*$^{-/-}$ mice, aged 3–5 months, was isolated using a standard surgical procedure. Following isolation, the muscle bundle was placed in Ca^{2+} free Tyrode's solution, 140 mM NaCl, 5 mM KCl, 2 mM $MgCl_2$, and 10 mM HEPES, pH 7.2. For muscle digestion, the same Tyrode's solution was supplemented with type II collagenase (Worthington) at a concentration of 2 mg/mL. Samples were digested by shaking for 120 min at 37°C. The digested muscle was dissociated by successive passages through pipettes of decreasing diameter. After the completion of muscle digestion, the isolated muscle fibers were plated onto MatTek glass-bottomed petri dishes in Tyrode's solution. No dissociation steps were taken to study membrane repair assay on intact muscle fibers. Membrane damage was induced in the presence of 2.5 μM FM4-64 amphiphilic fluorescent styryl pyridinium dye[18,48,54] (Invitrogen) and rhMG53 and BSA proteins with or without 2.0 mM Ca^{2+}, using the Olympus FV1000 multi-photon laser scanning confocal system. rhMG53 and BSA proteins were dissolved in saline solution and used in concentrations of 0.4 μM and 0.6 μM for individual fibers and whole muscle, respectively. A circular area was selected along the edge of the sarcolemma and irradiated at 24% of laser power for 3 s. Pre- and post-damage images were captured every 3 s,

continuing for 100 s. The extent of membrane damage was analyzed using ImageJ software, by measuring the fluorescence intensity encompassing the site of damage. To preclude any potential for bias, all of the experiments were performed in a blinded fashion.

Statistical Analysis

Results of the experiments were analyzed by the Student's t test or the Tukey and Benjamini, Krieger, and Yekutieli ANOVA methods using GraphPad Prism software (version 7.0). A threshold p value is indicated in the figures when statistical significance is determined for all groups as described in the individual figure legends, except where otherwise noted. All data are plotted as means ± SEM, except where otherwise described.

SUPPLEMENTAL INFORMATION

Supplemental Information includes five tables and can be found with this article online at http://dx.doi.org/10.1016/j.ymthe.2017.06.025.

AUTHOR CONTRIBUTIONS

N.W. and L.V.G. conceived and designed the overall study. L.V.G., K.E.M., J.A., and E.X.B. conducted animal studies and collected samples. S.B. conducted laser confocal microscopy measurements. L.V.G., K.E.M., and J.H.C. conducted downstream histological and biochemical analysis of samples. H.M. collected samples and conducted animal manipulations. N.W. and L.V.G. drafted the manuscript and E.X.B. contributed editing to the final manuscript.

CONFLICTS OF INTEREST

N.W. is a co-founder at TRIM-edicine, Inc, which is developing rhMG53 as a therapeutic strategy. Intellectual property relating to MG53 was patented by the Rutgers University Robert Wood Johnson Medical School.

ACKNOWLEDGMENTS

The Ohio State University's Pathology Core Facility (NIH National Cancer Institute support grant P30-CA016058) performed paraffin tissue processing. Images presented in this article were generated using the instruments and services at the Campus Microscopy and Imaging Facility, The Ohio State University. We also thank Dr. Louise Rodino-Klapac for providing the mouse monoclonal dysferlin antibody. This work was supported by a research grant from the Muscular Dystrophy Association (to N.W.) and an NIH National Institute of Arthritis and Musculoskeletal and Skin Diseases award (R01-AR063084 to N.W.). The content is solely the responsibility of the authors and does not necessarily represent the official views of the NIH. Further support was provided by the Center for Muscle Health and Neuromuscular Disorders (to L.V.G.) and an American Heart Association postdoctoral fellowship (14POST19990020 to L.V.G.).

REFERENCES

1. Bashir, R., Britton, S., Strachan, T., Keers, S., Vafiadaki, E., Lako, M., Richard, I., Marchand, S., Bourg, N., Argov, Z., et al. (1998). A gene related to Caenorhabditis elegans spermatogenesis factor fer-1 is mutated in limb-girdle muscular dystrophy type 2B. Nat. Genet. *20*, 37–42.

2. Illa, I., Serrano-Munuera, C., Gallardo, E., Lasa, A., Rojas-García, R., Palmer, J., Gallano, P., Baiget, M., Matsuda, C., and Brown, R.H. (2001). Distal anterior compartment myopathy: a dysferlin mutation causing a new muscular dystrophy phenotype. Ann. Neurol. *49*, 130–134.

3. Liu, J., Aoki, M., Illa, I., Wu, C., Fardeau, M., Angelini, C., Serrano, C., Urtizberea, J.A., Hentati, F., Hamida, M.B., et al. (1998). Dysferlin, a novel skeletal muscle gene, is mutated in Miyoshi myopathy and limb girdle muscular dystrophy. Nat. Genet. *20*, 31–36.

4. Ueyama, H., Kumamoto, T., Nagao, S., Masuda, T., Horinouchi, H., Fujimoto, S., and Tsuda, T. (2001). A new dysferlin gene mutation in two Japanese families with limb-girdle muscular dystrophy 2B and Miyoshi myopathy. Neuromuscul. Disord. *11*, 139–145.

5. Moore, S.A., Shilling, C.J., Westra, S., Wall, C., Wicklund, M.P., Stolle, C., Brown, C.A., Michele, D.E., Piccolo, F., Winder, T.L., et al. (2006). Limb-girdle muscular dystrophy in the United States. J. Neuropathol. Exp. Neurol. *65*, 995–1003.

6. Walter, M.C., Reilich, P., Thiele, S., Schessl, J., Schreiber, H., Reiners, K., Kress, W., Müller-Reible, C., Vorgerd, M., Urban, P., et al. (2013). Treatment of dysferlinopathy with deflazacort: a double-blind, placebo-controlled clinical trial. Orphanet J. Rare Dis. *8*, 26.

7. Aoki, M. (1993). Dysferlinopathy. In GeneReviews, R.A. Pagon, M.P. Adam, and H.H. Ardinger, eds. (Seattle: University of Washington) https://www.ncbi.nlm.nih.gov/books/NBK1303/.

8. Schoewel, V., Marg, A., Kunz, S., Overkamp, T., Carrazedo, R.S., Zacharias, U., Daniel, P.T., and Spuler, S. (2012). Dysferlin-peptides reallocate mutated dysferlin thereby restoring function. PLoS ONE *7*, e49603.

9. Turan, S., Farruggio, A.P., Srifa, W., Day, J.W., and Calos, M.P. (2016). Precise correction of disease mutations in induced pluripotent stem cells derived from patients with limb girdle muscular dystrophy. Mol. Ther. *24*, 685–696.

10. Angelini, C., Peterle, E., Gaiani, A., Bortolussi, L., and Borsato, C. (2011). Dysferlinopathy course and sportive activity: clues for possible treatment. Acta Myol. *30*, 127–132.

11. Pryadkina, M., Lostal, W., Bourg, N., Charton, K., Roudaut, C., Hirsch, M.L., and Richard, I. (2015). A comparison of AAV strategies distinguishes overlapping vectors for efficient systemic delivery of the 6.2 kb Dysferlin coding sequence. Mol. Ther. Methods Clin. Dev. *2*, 15009.

12. Sondergaard, P.C., Griffin, D.A., Pozsgai, E.R., Johnson, R.W., Grose, W.E., Heller, K.N., Shontz, K.M., Montgomery, C.L., Liu, J., Clark, K.R., et al. (2015). AAV.dysferlin overlap vectors restore function in dysferlinopathy animal models. Ann. Clin. Transl. Neurol. *2*, 256–270.

13. Vitale, J.M., Schneider, J.S., Beck, A.J., Zhao, Q., Chang, C., Gordan, R., Michaels, J., Bhaumik, M., and Fraidenraich, D. (2012). Dystrophin-compromised sarcoglycan-δ-knockout diaphragm requires full wild-type embryonic stem cell reconstitution for correction. J. Cell Sci. *125*, 1807–1813.

14. Merrick, D., Stadler, L.K., Larner, D., and Smith, J. (2009). Muscular dystrophy begins early in embryonic development deriving from stem cell loss and disrupted skeletal muscle formation. Dis. Model. Mech. *2*, 374–388.

15. Kong, K.Y., Ren, J., Kraus, M., Finklestein, S.P., and Brown, R.H., Jr. (2004). Human umbilical cord blood cells differentiate into muscle in sjl muscular dystrophy mice. Stem Cells *22*, 981–993.

16. Ampong, B.N., Imamura, M., Matsumiya, T., Yoshida, M., and Takeda, S. (2005). Intracellular localization of dysferlin and its association with the dihydropyridine receptor. Acta Myol. *24*, 134–144.

17. Anderson, L.V., Davison, K., Moss, J.A., Young, C., Cullen, M.J., Walsh, J., Johnson, M.A., Bashir, R., Britton, S., Keers, S., et al. (1999). Dysferlin is a plasma membrane protein and is expressed early in human development. Hum. Mol. Genet. *8*, 855–861.

18. Bansal, D., Miyake, K., Vogel, S.S., Groh, S., Chen, C.C., Williamson, R., McNeil, P.L., and Campbell, K.P. (2003). Defective membrane repair in dysferlin-deficient muscular dystrophy. Nature *423*, 168–172.

19. Bansal, D., and Campbell, K.P. (2004). Dysferlin and the plasma membrane repair in muscular dystrophy. Trends Cell Biol. *14*, 206–213.

20. Chase, T.H., Cox, G.A., Burzenski, L., Foreman, O., and Shultz, L.D. (2009). Dysferlin deficiency and the development of cardiomyopathy in a mouse model of limb-girdle muscular dystrophy 2B. Am. J. Pathol. *175*, 2299–2308.

21. Han, R., Bansal, D., Miyake, K., Muniz, V.P., Weiss, R.M., McNeil, P.L., and Campbell, K.P. (2007). Dysferlin-mediated membrane repair protects the heart from stress-induced left ventricular injury. J. Clin. Invest. *117*, 1805–1813.

22. Glover, L., and Brown, R.H., Jr. (2007). Dysferlin in membrane trafficking and patch repair. Traffic *8*, 785–794.

23. Wallace, G.Q., and McNally, E.M. (2009). Mechanisms of muscle degeneration, regeneration, and repair in the muscular dystrophies. Annu. Rev. Physiol. *71*, 37–57.

24. McNeil, P.L., and Steinhardt, R.A. (2003). Plasma membrane disruption: repair, prevention, adaptation. Annu. Rev. Cell Dev. Biol. *19*, 697–731.

25. McNeil, P.L., Vogel, S.S., Miyake, K., and Terasaki, M. (2000). Patching plasma membrane disruptions with cytoplasmic membrane. J. Cell Sci. *113*, 1891–1902.

26. Covian-Nares, J.F., Koushik, S.V., Puhl, H.L., 3rd, and Vogel, S.S. (2010). Membrane wounding triggers ATP release and dysferlin-mediated intercellular calcium signaling. J. Cell Sci. *123*, 1884–1893.

27. de Morrée, A., Hensbergen, P.J., van Haagen, H.H., Dragan, I., Deelder, A.M., 't Hoen, P.A., Frants, R.R., and van der Maarel, S.M. (2010). Proteomic analysis of the dysferlin protein complex unveils its importance for sarcolemmal maintenance and integrity. PLoS ONE *5*, e13854.

28. Demonbreun, A.R., Fahrenbach, J.P., Deveaux, K., Earley, J.U., Pytel, P., and McNally, E.M. (2011). Impaired muscle growth and response to insulin-like growth factor 1 in dysferlin-mediated muscular dystrophy. Hum. Mol. Genet. *20*, 779–789.

29. Evesson, F.J., Peat, R.A., Lek, A., Brilot, F., Lo, H.P., Dale, R.C., Parton, R.G., North, K.N., and Cooper, S.T. (2010). Reduced plasma membrane expression of dysferlin mutants is attributed to accelerated endocytosis via a syntaxin-4-associated pathway. J. Biol. Chem. *285*, 28529–28539.

30. Han, R., Frett, E.M., Levy, J.R., Rader, E.P., Lueck, J.D., Bansal, D., Moore, S.A., Ng, R., Beltrán-Valero de Bernabé, D., Faulkner, J.A., and Campbell, K.P. (2010). Genetic ablation of complement C3 attenuates muscle pathology in dysferlin-deficient mice. J. Clin. Invest. *120*, 4366–4374.

31. Nagaraju, K., Rawat, R., Veszelovszky, E., Thapliyal, R., Kesari, A., Sparks, S., Raben, N., Plotz, P., and Hoffman, E.P. (2008). Dysferlin deficiency enhances monocyte phagocytosis: a model for the inflammatory onset of limb-girdle muscular dystrophy 2B. Am. J. Pathol. *172*, 774–785.

32. Wenzel, K., Carl, M., Perrot, A., Zabojszcza, J., Assadi, M., Ebeling, M., Geier, C., Robinson, P.N., Kress, W., Osterziel, K.J., and Spuler, S. (2006). Novel sequence variants in dysferlin-deficient muscular dystrophy leading to mRNA decay and possible C2-domain misfolding. Hum. Mutat. *27*, 599–600.

33. Wenzel, K., Zabojszcza, J., Carl, M., Taubert, S., Lass, A., Harris, C.L., Ho, M., Schulz, H., Hummel, O., Hubner, N., et al. (2005). Increased susceptibility to complement attack due to down-regulation of decay-accelerating factor/CD55 in dysferlin-deficient muscular dystrophy. J. Immunol. *175*, 6219–6225.

34. Kerr, J.P., Ziman, A.P., Mueller, A.L., Muriel, J.M., Kleinhans-Welte, E., Gumerson, J.D., Vogel, S.S., Ward, C.W., Roche, J.A., and Bloch, R.J. (2013). Dysferlin stabilizes stress-induced Ca2+ signaling in the transverse tubule membrane. Proc. Natl. Acad. Sci. USA *110*, 20831–20836.

35. Kuru, S., Yasuma, F., Wakayama, T., Kimura, S., Konagaya, M., Aoki, M., Tanabe, M., and Takahashi, T. (2004). [A patient with limb girdle muscular dystrophy type 2B (LGMD2B) manifesting cardiomyopathy]. Rinsho Shinkeigaku *44*, 375–378.

36. Wenzel, K., Geier, C., Qadri, F., Hubner, N., Schulz, H., Erdmann, B., Gross, V., Bauer, D., Dechend, R., Dietz, R., et al. (2007). Dysfunction of dysferlin-deficient hearts. J. Mol. Med. (Berl.) *85*, 1203–1214.

37. Choi, E.R., Park, S.J., Choe, Y.H., Ryu, D.R., Chang, S.A., Choi, J.O., Lee, S.C., Park, S.W., Kim, B.J., Kim, D.K., and Oh, J.K. (2010). Early detection of cardiac involvement in Miyoshi myopathy: 2D strain echocardiography and late gadolinium enhancement cardiovascular magnetic resonance. J. Cardiovasc. Magn. Reson. *12*, 31.

38. Ho, M., Post, C.M., Donahue, L.R., Lidov, H.G., Bronson, R.T., Goolsby, H., Watkins, S.C., Cox, G.A., and Brown, R.H., Jr. (2004). Disruption of muscle membrane and phenotype divergence in two novel mouse models of dysferlin deficiency. Hum. Mol. Genet. *13*, 1999–2010.

39. Lostal, W., Bartoli, M., Roudaut, C., Bourg, N., Krahn, M., Pryadkina, M., Borel, P., Suel, L., Roche, J.A., Stockholm, D., et al. (2012). Lack of correlation between outcomes of membrane repair assay and correction of dystrophic changes in experimental therapeutic strategy in dysferlinopathy. PLoS ONE *7*, e38036.

40. Barthélémy, F., Wein, N., Krahn, M., Lévy, N., and Bartoli, M. (2011). Translational research and therapeutic perspectives in dysferlinopathies. Mol. Med. *17*, 875–882.

41. Fuson, K., Rice, A., Mahling, R., Snow, A., Nayak, K., Shanbhogue, P., Meyer, A.G., Redpath, G.M., Hinderliter, A., Cooper, S.T., and Sutton, R.B. (2014). Alternate splicing of dysferlin C2A confers Ca^{2+}-dependent and Ca^{2+}-independent binding for membrane repair. Structure *22*, 104–115.

42. Vafiadaki, E., Reis, A., Keers, S., Harrison, R., Anderson, L.V., Raffelsberger, T., Ivanova, S., Hoger, H., Bittner, R.E., Bushby, K., and Bashir, R. (2001). Cloning of the mouse dysferlin gene and genomic characterization of the SJL-Dysf mutation. Neuroreport *12*, 625–629.

43. Bittner, R.E., Anderson, L.V., Burkhardt, E., Bashir, R., Vafiadaki, E., Ivanova, S., Raffelsberger, T., Maerk, I., Höger, H., Jung, M., et al. (1999). Dysferlin deletion in SJL mice (SJL-Dysf) defines a natural model for limb girdle muscular dystrophy 2B. Nat. Genet. *23*, 141–142.

44. Lostal, W., Bartoli, M., Bourg, N., Roudaut, C., Bentaïb, A., Miyake, K., Guerchet, N., Fougerousse, F., McNeil, P., and Richard, I. (2010). Efficient recovery of dysferlin deficiency by dual adeno-associated vector-mediated gene transfer. Hum. Mol. Genet. *19*, 1897–1907.

45. Blazek, A.D., Paleo, B.J., and Weisleder, N. (2015). Plasma membrane repair: a central process for maintaining cellular homeostasis. Physiology (Bethesda) *30*, 438–448.

46. Meroni, G., and Diez-Roux, G. (2005). TRIM/RBCC, a novel class of 'single protein RING finger' E3 ubiquitin ligases. BioEssays *27*, 1147–1157.

47. Weisleder, N., Takeshima, H., and Ma, J. (2009). Mitsugumin 53 (MG53) facilitates vesicle trafficking in striated muscle to contribute to cell membrane repair. Commun. Integr. Biol. *2*, 225–226.

48. Cai, C., Masumiya, H., Weisleder, N., Matsuda, N., Nishi, M., Hwang, M., Ko, J.K., Lin, P., Thornton, A., Zhao, X., et al. (2009). MG53 nucleates assembly of cell membrane repair machinery. Nat. Cell Biol. *11*, 56–64.

49. Cai, C., Masumiya, H., Weisleder, N., Pan, Z., Nishi, M., Komazaki, S., Takeshima, H., and Ma, J. (2009). MG53 regulates membrane budding and exocytosis in muscle cells. J. Biol. Chem. *284*, 3314–3322.

50. Cai, C., Weisleder, N., Ko, J.K., Komazaki, S., Sunada, Y., Nishi, M., Takeshima, H., and Ma, J. (2009). Membrane repair defects in muscular dystrophy are linked to altered interaction between MG53, caveolin-3, and dysferlin. J. Biol. Chem. *284*, 15894–15902.

51. Masumiya, H., Asaumi, Y., Nishi, M., Minamisawa, S., Adachi-Akahane, S., Yoshida, M., Kangawa, K., Ito, K., Kagaya, Y., Yanagisawa, T., et al. (2009). Mitsugumin 53-mediated maintenance of K+ currents in cardiac myocytes. Channels (Austin) *3*, 6–11.

52. Liu, J., Zhu, H., Zheng, Y., Xu, Z., Li, L., Tan, T., Park, K.H., Hou, J., Zhang, C., Li, D., et al. (2015). Cardioprotection of recombinant human MG53 protein in a porcine model of ischemia and reperfusion injury. J. Mol. Cell. Cardiol. *80*, 10–19.

53. Weisleder, N., Lin, P., Zhao, X., Orange, M., Zhu, H., and Ma, J. (2011). Visualization of MG53-mediated cell membrane repair using in vivo and in vitro systems. J. Vis. Exp. *12*, 31.

54. Weisleder, N., Takizawa, N., Lin, P., Wang, X., Cao, C., Zhang, Y., Tan, T., Ferrante, C., Zhu, H., Chen, P.J., et al. (2012). Recombinant MG53 protein modulates therapeutic cell membrane repair in treatment of muscular dystrophy. Sci. Transl. Med. *4*, 139ra85.

55. de Luna, N., Gallardo, E., Soriano, M., Dominguez-Perles, R., de la Torre, C., Rojas-García, R., García-Verdugo, J.M., and Illa, I. (2006). Absence of dysferlin alters myogenin expression and delays human muscle differentiation "in vitro". J. Biol. Chem. *281*, 17092–17098.

56. De Palma, S., Morandi, L., Mariani, E., Begum, S., Cerretelli, P., Wait, R., and Gelfi, C. (2006). Proteomic investigation of the molecular pathophysiology of dysferlinopathy. Proteomics *6*, 379–385.

57. Diers, A., Carl, M., Stoltenburg-Didinger, G., Vorgerd, M., and Spuler, S. (2007). Painful enlargement of the calf muscles in limb girdle muscular dystrophy

type 2B (LGMD2B) with a novel compound heterozygous mutation in DYSF. Neuromuscul. Disord. *17*, 157–162.

58. Barton, E.R., Wang, B.J., Brisson, B.K., and Sweeney, H.L. (2010). Diaphragm displays early and progressive functional deficits in dysferlin-deficient mice. Muscle Nerve *42*, 22–29.

59. Bönnemann, C.G., and Finkel, R.S. (2002). Sarcolemmal proteins and the spectrum of limb-girdle muscular dystrophies. Semin. Pediatr. Neurol. *9*, 81–99.

60. Alloush, J., and Weisleder, N. (2013). TRIM proteins in therapeutic membrane repair of muscular dystrophy. JAMA Neurol. *70*, 928–931.

61. McNeil, P.L., and Kirchhausen, T. (2005). An emergency response team for membrane repair. Nat. Rev. Mol. Cell Biol. *6*, 499–505.

62. Miyake, K., and McNeil, P.L. (1995). Vesicle accumulation and exocytosis at sites of plasma membrane disruption. J. Cell Biol. *131*, 1737–1745.

63. Armstrong, R.B., Ogilvie, R.W., and Schwane, J.A. (1983). Eccentric exercise-induced injury to rat skeletal muscle. J. Appl. Physiol. *54*, 80–93.

64. Brancaccio, P., Maffulli, N., and Limongelli, F.M. (2007). Creatine kinase monitoring in sport medicine. Br. Med. Bull. *81-82*, 209–230.

65. Rossi, C.A., Pozzobon, M., Ditadi, A., Archacka, K., Gastaldello, A., Sanna, M., Franzin, C., Malerba, A., Milan, G., Cananzi, M., et al. (2010). Clonal characterization of rat muscle satellite cells: proliferation, metabolism and differentiation define an intrinsic heterogeneity. PLoS ONE *5*, e8523.

66. Terrill, J.R., Radley-Crabb, H.G., Grounds, M.D., and Arthur, P.G. (2012). N-Acetylcysteine treatment of dystrophic mdx mice results in protein thiol modifications and inhibition of exercise induced myofibre necrosis. Neuromuscul. Disord. *22*, 427–434.

67. Reid, M.B., Lännergren, J., and Westerblad, H. (2002). Respiratory and limb muscle weakness induced by tumor necrosis factor-alpha: involvement of muscle myofilaments. Am. J. Respir. Crit. Care Med. *166*, 479–484.

68. Demonbreun, A.R., Allen, M.V., Warner, J.L., Barefield, D.Y., Krishnan, S., Swanson, K.E., Earley, J.U., and McNally, E.M. (2016). Enhanced muscular dystrophy from loss of dysferlin is accompanied by impaired annexin A6 translocation after sarcolemmal disruption. Am. J. Pathol. *186*, 1610–1622.

69. Hwang, M., Ko, J.K., Weisleder, N., Takeshima, H., and Ma, J. (2011). Redox-dependent oligomerization through a leucine zipper motif is essential for MG53-mediated cell membrane repair. Am. J. Physiol. Cell Physiol. *301*, C106–C114.

70. Ma, H., Liu, J., Bian, Z., Cui, Y., Zhou, X., Zhou, X., Zhang, B., Adesanya, T.M., Yi, F., Park, K.H., et al. (2015). Effect of metabolic syndrome on mitsugumin 53 expression and function. PLoS ONE *10*, e0124128.

71. Judson, R.N., Gray, S.R., Walker, C., Carroll, A.M., Itzstein, C., Lionikas, A., Zammit, P.S., De Bari, C., and Wackerhage, H. (2013). Constitutive expression of Yes-associated protein (Yap) in adult skeletal muscle fibres induces muscle atrophy and myopathy. PLoS ONE *8*, e59622.

72. Hamer, P.W., McGeachie, J.M., Davies, M.J., and Grounds, M.D. (2002). Evans blue dye as an in vivo marker of myofibre damage: optimising parameters for detecting initial myofibre membrane permeability. J. Anat. *200*, 69–79.

73. Jia, Y., Chen, K., Lin, P., Lieber, G., Nishi, M., Yan, R., Wang, Z., Yao, Y., Li, Y., Whitson, B.A., et al. (2014). Treatment of acute lung injury by targeting MG53-mediated cell membrane repair. Nat. Commun. *5*, 4387.

74. Kim, S., Seo, J., Ko, Y.G., Huh, Y.D., and Park, H. (2012). Lipid-binding properties of TRIM72. BMB Rep. *45*, 26–31.

75. Cárdenas, A.M., González-Jamett, A.M., Cea, L.A., Bevilacqua, J.A., and Caviedes, P. (2016). Dysferlin function in skeletal muscle: possible pathological mechanisms and therapeutical targets in dysferlinopathies. Exp. Neurol. *283* (Pt A), 246–254.

76. Klinge, L., Harris, J., Sewry, C., Charlton, R., Anderson, L., Laval, S., Chiu, Y.H., Hornsey, M., Straub, V., Barresi, R., et al. (2010). Dysferlin associates with the developing T-tubule system in rodent and human skeletal muscle. Muscle Nerve *41*, 166–173.

77. Demonbreun, A.R., Rossi, A.E., Alvarez, M.G., Swanson, K.E., Deveaux, H.K., Earley, J.U., Hadhazy, M., Vohra, R., Walter, G.A., Pytel, P., and McNally, E.M. (2014). Dysferlin and myoferlin regulate transverse tubule formation and glycerol sensitivity. Am. J. Pathol. *184*, 248–259.

78. Ahn, M.K., Lee, K.J., Cai, C., Huang, M., Cho, C.H., Ma, J., and Lee, E.H. (2016). Mitsugumin 53 regulates extracellular Ca(2+) entry and intracellular Ca(2+) release via Orai1 and RyR1 in skeletal muscle. Sci. Rep. *6*, 36909.

79. Weisleder, N., Ferrante, C., Hirata, Y., Collet, C., Chu, Y., Cheng, H., Takeshima, H., and Ma, J. (2007). Systemic ablation of RyR3 alters Ca2+ spark signaling in adult skeletal muscle. Cell Calcium *42*, 548–555.

YMTHE, Volume *25*

Supplemental Information

Treatment with Recombinant Human MG53 Protein Increases Membrane Integrity in a Mouse Model of Limb Girdle Muscular Dystrophy 2B

Liubov V. Gushchina, Sayak Bhattacharya, Kevin E. McElhanon, Jin Hyuk Choi, Heather Manring, Eric X Beck, Jenna Alloush, and Noah Weisleder

Supplemental Information for Gushchina, et al.

Supplementary Table S1. Statistical analysis of histological features of muscular dystrophy in *Dysf*$^{-/-}$ mice.

Skeletal Muscle	*P value (3 vs 6 months)*	*P value (3 vs 10-12 months)*	*P value (3 vs 15-16 months)*	*P value (6 vs 10-12 months)*	*P value (6 vs 15-16 months)*	*P value (10-12 vs 15-16 months)*
Histopathological area						
Gluteus	n/s	0.0019	<0.0001	0.0069	0.0002	n/s
Gastroc	n/s	n/s	0.0021	n/s	0.0027	0.0003
Central Nuclei						
Gluteus	n/s	<0.0001	<0.0001	<0.0001	<0.0001	n/s
Gastroc	n/s	n/s	<0.0001	n/s	<0.0001	<0.0001

n/s – measurements are not significantly different

P values are calculated by *Tukey-ANOVA* method using Prism software (GraphPad Prism 7.0, USA).

Supplementary Table S2. Statistical analysis of *ex vivo* studies of rhMG53 efficacy on whole FDB muscle derived from *Dysf*$^{-/-}$ mice.

	P value (Dysf KO, Saline, 2 mM Ca^{2+})	*P value* (Dysf KO, BSA, 0 mM Ca^{2+})	*P value* (Dysf KO, BSA, 2 mM Ca^{2+})	*P value* (Dysf KO, rhMG53, 0 mM Ca^{2+})	*P value* (Dysf KO, rhMG53, 2 mM Ca^{2+})	*P value* (WT 0 mM Ca^{2+})
AUC						
Dysf KO,	<0.0001	<0.0001	<0.0001	n/s	n/s	n/s

rhMG53, 0 mM Ca^{2+}						
Dysf KO, rhMG53, 2 mM Ca^{2+}	<0.0001	<0.0001	<0.0001	n/s	n/s	n/s
WT 0 mM Ca^{2+}	0.0006	n/s	n/s	<0.0001	<0.0001	n/s
WT 2 mM Ca^{2+}	<0.0001	<0.0001	<0.0001	n/s	n/s	<0.0001
MaxFluor FM4-64						
Dysf KO, rhMG53, 0 mM Ca^{2+}	<0.0001	<0.0001	<0.0001	n/s	n/s	n/s
Dysf KO, rhMG53, 2 mM Ca^{2+}	<0.0001	<0.0001	<0.0001	n/s	n/s	n/s
WT 0 mM Ca^{2+}	n/s	n/s	n/s	<0.0001	<0.0001	n/s
WT 2 mM Ca^{2+}	<0.0001	<0.0001	<0.0001	n/s	n/s	<0.0001

n/s – measurements are not significantly different

P values are calculated by *Tukey-ANOVA* method using Prism software (GraphPad Prism 7.0, USA).

Supplementary Table S3. Effect of serum CK and LDH release in *Dysf*$^{-/-}$ mice after treatment and downhill running exercise.

	CK level (IU/L)	**LDH level (IU*10^3/L)**
WT (C57BL/6J)	17.7 ± 4.6	55.0 ± 3.2
Dysf$^{-/-}$ Sedentary (control)	58.5 ± 6.4	76.5 ± 3.2
Dysf$^{-/-}$ Pre-exercise-Saline	67.6 ± 6.7	88.7 ± 5.6
Dysf$^{-/-}$ Post-exercise-Saline	157.5 ± 14.8	148.9 ± 15.4
Dysf$^{-/-}$ Pre-exercise-rhMG53	67.0 ± 9.8	74.5 ± 11.4
Dysf$^{-/-}$ Post-exercise-rhMG53	123.0 ± 8.0	120.1 ± 12.1

Supplementary Table S4. Quantification analysis of IgG positive fibers from *Dysf*$^{-/-}$ mice.

Muscle	**Control***	**Post-exercise-Saline***	**Post-exercise-rhMG53***
Gluteus	7.9 ± 1.4	17.7 ± 1.8	13.1 ± 1.4
EDL	24.3 ± 1.1	29.8 ± 1.3	26.3 ± 1.0
Soleus	11.6 ± 1.3	18.5 ± 1.1	13.5 ± 0.8

*The quantification result was expressed as the mean of positive fibers to the total number of fibers ratio, expressed as a percentage.

Supplementary Table S5. Absorption spectroscopy analysis of EBD-injected *Dysf*$^{-/-}$ mice after treatment and downhill running exercise.

Muscle	Control*	Post-exercise-Saline*	Post-exercise-rhMG53*
Gluteus	2.5 ± 0.13	3.2 ± 0.12	2.9 ± 0.14
Soleus	5.2 ± 0.17	6.0 ± 0.29	5.3 ± 0.21
EDL	2.5 ± 0.15	3.4 ± 0.19	2.7 ± 0.10
TA	1.7 ± 0.09	2.4 ± 0.17	2.2 ± 0.06
Gastroc	2.0 ± 0.10	2.6 ± 0.14	2.4 ± 0.05
FDB	5.5 ± 0.59	5.4 ± 0.48	5.5 ± 0.62
Diaphragm	8.2 ± 0.18	8.4 ± 0.21	8.5 ± 0.26
Kidney	11.4 ± 0.40	13.7 ± 0.48	13.5 ± 0.43

*The absorption results of EBD uptake were expressed as the mean of $OD^{(620-800)}$/tissue (g).